Article

Incorporation of Microgrid Technology Solutions to Reduce Power Loss in a Distribution Network with Elimination of Inefficient Power Conversion Strategies

Mageswaran Rengasamy [1,*]**, Sivasankar Gangatharan** [1]**, Rajvikram Madurai Elavarasan** [1] **and Lucian Mihet-Popa** [2,*]

[1] Department of Electrical and Electronics Engineering, Thiagarajar College of Engineering, Madurai 625015, India; gsivasankar@tce.edu (S.G.); rajvikram787@gmail.com (R.M.E.)
[2] Faculty of Information Technology, Engineering and Economics, Oestfold University College, 1757 Halden, Norway
[*] Correspondence: mageswaranrr@gmail.com (M.R.); lucian.mihet@hiof.no (L.M.-P.)

Abstract: The increase in energy-efficient DC appliances and electronic gadgets has led to an upheaval in the usage of AC–DC power convertors; hence, power loss in converter devices is cumulatively increasing. Evolving microgrid technology has also become deeply integrated with the conversion process due to increased power converters in its infrastructure, significantly worsening the power loss situation. One of the practical solutions to this disturbance is to reduce conversion losses in domestic distribution systems through the optimal deployment of the battery storage system and solar PV power using microgrid technology. In this paper, a novel energy management system is developed that uses a new control algorithm, termed Inefficient Power Conversion Elimination Algorithm (IPCEA). The proposed algorithm compares the Net Transferable Power (NTP) available on the DC side with the loss rate across the converter. The converter is switched off (or disconnected from the grid and load) if the NTP is less than 20% of the converter rating to avoid low-efficiency power conversion. The solar PV system is connected to the DC bus to supply the DC loads while the AC loads are supplied from the AC source (utility power). An auxiliary battery pack is integrated to the DC side to feed DC loads during the absence of solar energy. A battery energy storage system (BESS) is deployed to manage energy distribution effectively. The power distribution is managed using a centralized microgrid controller, and the load demand is met accordingly. Thereby, the power generated by the solar PV can be utilized effectively. Microgrid technology's effectiveness is emphasized by comparative analysis, and the achievements are discussed in detail and highlighted using a prototype model.

Keywords: renewable energy; AC/DC microgrid; automatic centralized microgrid; controller algorithm; distribution system

1. Introduction

DC appliances are receiving increasing attention due to their energy efficiency [1,2]. However, DC appliances are connected to the AC supply through power electronic convert-ers and these convertors introduce numerous nonlinearity and conversion losses into the system. On the other hand, microgrid technology is developed to efficiently manage the power supply from renewable energy sources and energy storage systems [3,4]. Current research is focused on the optimization of distributed generation systems connected to mi-crogrids to meet the load demand with reduced electricity costs [5]. Microgrid technology has been deployed to perform demand-side management to reduce the Peak-to-Average Ratio and increase financial savings to satisfy consumers [6]. In spite of its several ad-vantageous features, the microgrids consist of several power electronic converters; the conversion losses become a crucial drawback. In [7], a new controller for the string stability

of the microgrid inverter has been proposed to improve its performance. The authors of one study [8] proposed a solid-state DC transformer to reduce the number of switching devices on the DC link; consequently, device losses have reduced. The interoperability and extensibility features of distributed energy sources are enhanced by incorporating advanced Smart Microgrid energy management techniques [9]. However, a serious issue arises when topologies are constructed with converters working at low efficiency during power conversion [10,11].

Microgrid technology used for distributed generation systems often performs power conversion at low efficiency and suffers huge conversion losses cumulatively [12,13]. These losses cannot be quantified because the efficiency of the converters is highly nonlinear [14] and their efficiency fluctuates with the variation in load as well as operating temperature. The power conversion between AC and DC buses is efficient only if the power available for transfer is equivalent to its rating. However, in real time, the power available for conversion is not always concordant with the power rating and at under-loaded conditions; inefficient conversion occurs, which results in increased power loss across the converters. Similarly, when the DC bus requires less power, invoking a converter to draw power from the AC bus might be inefficient [15]. Ignoring this power conversion results in an inefficient process. Although individual power convertor loss is less, when considered on a large scale, cumulative losses reach a prodigious value. In this proposed study, the phenomenon of inefficient power conversion due to the underperformance of convertors at under-loaded conditions is referred to as inefficient power. Generally, research has not focused on the elimination of inefficient power conversion processes. The authors of this study have already carried out extensive research in this domain and accomplished various research objectives, such as the mitigation of power conversion loss, as in [16], and cost minimization, as in [17]. In this study, an exclusive conversion loss reduction and cost minimization strategy is explored and designed based on a novel control algorithm, named Inefficient Power Conversion Elimination Algorithm (IPCEA), using a battery energy storage system (BESS).

The study proposes the design of a novel switching strategy to incorporate a hybrid microgrid in the distribution system effectively. It comprises the following conventional electrical installation, with an intelligent microgrid distribution system:

i. To implement a renewable-based IPCEA considering the availability of Net Transferable Power (NTP) at DC bus and the rate of converter loss to minimize low-efficiency power conversion.
ii. To effectively manage battery energy within the DC side of the microgrid to minimize the charge cycle and improve its performance.
iii. To decrease the stress on the utility grid by reducing the rate of power exchange.

2. An Overview of the Conversion Losses in Various Distribution System Components

The advancement in semiconductor technology underpins the invention of a variety of energy-efficient equipment. Although these devices are energy-efficient, they distort the current profile and exhibit conversion loss in the system to which they are connected. Consequently, the increased usage of battery backup, consisting of different varieties of converters, further questions the current characteristics as well as power quality standards. Globally, several countries promote energy storage systems through subsidies to help increase storage potential. Consequently, the converter used for the battery backup system also causes several issues, among which conversion loss is one of the major concerns that requires significant focus.

2.1. Influence of Transformer Performance

The efficiency of a transformer is greater than 90% and remains constant when it is loaded to more than 20% of its rating [18]. The transformer exhibits poor efficiency during under-loaded conditions because of constant iron loss, and the efficiency is reduced due to

an increase in the copper loss at overload conditions [19,20]. Further, the reactive current is drawn under light load conditions and leads to a reactive power increase. The efficiency expression of the distribution transformer is furnished below.

$$\eta = \frac{V_2 I_2\ cos\Phi}{V_2 I_2\ cos\Phi + P_i + x^2 P_c} \tag{1}$$

where

$$x = \sqrt{\frac{P_i}{P_c}}$$

V_2—Secondary side voltage
I_2—Secondary side current
P_i—Iron loss
P_c—Copper loss
$Cos\Phi$—Power Factor

2.2. Impact of Inverter Losses

An inverter used in a domestic distribution system operates at a maximum efficiency of approximately 85% when it is loaded above 75% of its rating. The system features low efficiency in under-loaded conditions and it can even decrease to 50% when it is lightly loaded [21,22]. In addition, frequent conversion at under-loaded conditions results in sizeable power losses. The inverter loss accounts for switching and conduction losses. The inverter losses are calculated using the following expressions:

The IGBT comprises an IGBT switch with anti-parallel diode. Hence, the total loss in the switch is expressed as

$$P_{tot\ loss} = P_{IGBT\ loss} + P_{Diode\ loss} \tag{2}$$

where

$P_{tot\ loss}$—Total power loss
$P_{IGBT\ loss}$—Power loss due to IGBT switch

The loss in the IGBT switch is due to conduction loss and switching loss and it is expressed as

$$P_{IGBT\ loss} = P_{Cond} + P_{sw} \tag{3}$$

where

P_{Cond}—Power loss during conduction
P_{sw}—Power loss due to switching

The conduction loss is derived from the voltage across the collector and emitter terminals of the IGBT switch and current between its terminals. It is expressed as

$$P_{cond(I)} = \frac{1}{T_C} \int_0^{T_C} [Vce(t) \times I_{ce}(t)]\ dt \tag{4}$$

where

V_{CE}—Collector-to-emitter voltage of IGBT switch
I_{CE}—Collector-to-emitter current of IGBT switch

The switching loss occurs when the switch is turned ON and OFF. It increases in line with increases in the switching frequency. It is expressed as

$$P_{sw(I)} = f_{sw} * \left(E_{on} + E_{off} \right) \tag{5}$$

where

f_{sw}—Switching Frequency
E_{on}—Energy loss during IGBT ON state
E_{off}—Energy loss during IGBT OFF state

$$P_{Diode\ loss} = P_{sw(D)} = f_{sw} * (E_{on} + E_{rr}) \tag{6}$$

where

E_{rr}—Reverse recovery energy loss

To understand the actual losses, the efficiency characteristics of a real-time inverter were obtained through experiments. The specification of the inverter is summarized in Appendix A. The performance characteristics of the inverter are depicted in Figure 1. The performance of the inverter was obtained from the characteristic curve in this study. The inverter shows an efficiency of 85% during full load condition and it drops drastically to 50% when it is under-loaded. Similar work has been discussed in [23].
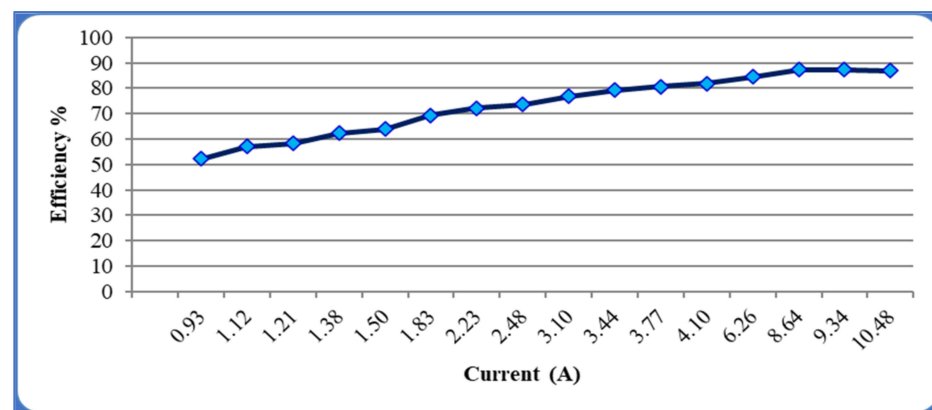
Figure 1. Performance characteristics of the inverter.

2.3. Influence of BESS

The battery efficiency is generally 85%, and the 15% shortfall is due to the losses in the charging and discharging process [24,25]. The efficiency further drops if the charges are stored for a long duration, where the self-discharge occurs due to internal resistance.

$$R_{int} = \left(\frac{V_{NL}}{V_{FL}} - 1\right) R_L \tag{7}$$

where

R_{int}—Internal resistance
V_{NL}—No load Voltage
V_{FL}—Full load voltage
R_L—Load resistance

The actual discharge time is given as

$$t = H\left(\frac{C}{IH}\right)^k \tag{8}$$

where

H—Time of discharge
C—Rate of discharge
I—Current discharge
k—Peukert constant (1.1 to 1.3)

Energy Efficiency is given as

$$\eta = \frac{E_D}{E_C} = \frac{\textit{Energy during discharging}}{\textit{Energy during charging}} = \frac{V_D I_D T_D}{V_C I_C T_C} \tag{9}$$

where

η—Energy Efficiency
E_D—Energy during discharge
E_C—Energy during charge
V_D—Diode voltage
I_D—Diode Current
T_D—Discharge time
V_C—Capacitor voltage
I_C—Capacitor current
T_C—Charging time

When the battery is charged from the utility, the power flows through the transformer, converters, and respective filters. As a result, the performance of all the equipment connected to the power supply line exerts an influence on the performance of the battery storage system. Hence, the capacity of the battery deteriorates. The battery capacity can be expressed as

$$C_B = \frac{L_D * A}{P_D * \eta_{trs} * \eta_{inv} * \eta_{cc}} \tag{10}$$

where $L_D = \frac{E_D}{V}$

C_B—Required capacity of the battery bank
L_D—Load demand
A—Autonomy days
P_D—Depth of discharge of the selected battery
η_{trs}—Transformer efficiency
η_{inv}—Efficiency of the inverter
η_{cc}—Efficiency of the charge controller
E_D—Estimated Energy demand

3. Inefficient Power Conversion Scenario Prevailing in the Distribution System

Theoretically, the maximum efficiency of the battery is claimed as 85% in previous research, but in the actual battery, the charging efficiency is determined by the power supply strategy. In many scenarios, a greater amount of power is lost in the conversion processes than expected. In this context, inefficient power conversion is one of the strategies in which the discharge of battery energy occurs in the most inefficient way. Various power distribution schemes and associated conversion losses are discussed in the following subsection.

3.1. Scheme 1: Battery Storage Systems Used as a Backup

Generally, batteries are used as a power backup component in residential premises, as shown in Figure 2. The system comprises a bidirectional converter, a transformer, and a battery, whose power rating depends on the backup duration and load requirement. This set of equipment exhibits considerable losses. These losses are higher if the system is under-loaded.
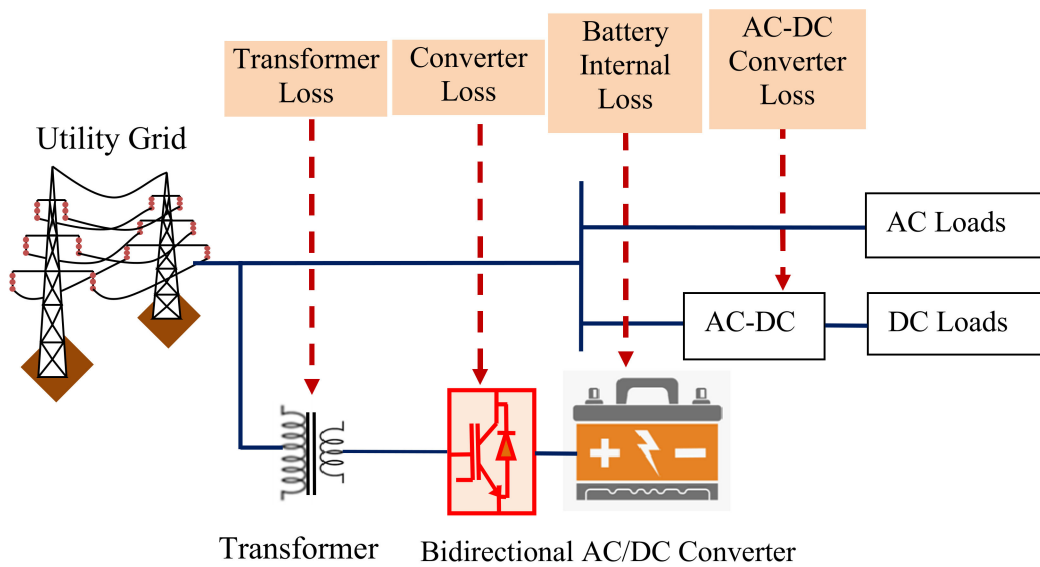
Figure 2. The battery storage system used in conventional system.

The transformer loss is expressed as

$$P_{\text{trs, loss}} = P_i + P_c \tag{11}$$

where

P_i = Core loss
P_c = Copper loss

The losses across the inverter are expressed as

$$P_{\text{inv,loss}} = P_{\text{AC.PT}} \left(\frac{1}{\eta_{\text{inv}}} - 1 \right) \tag{12}$$

where

$P_{\text{inv,loss}}$ = Inverter loss
$P_{\text{AC.PT}}$ = Power transferred to AC loads through inverter
η_{inv} = Inverter efficiency

The battery internal loss is expressed as

$$P_{\text{B.int,loss}} = i_{\text{BT}}^2 R_{\text{B.int}} \tag{13}$$

where

$P_{\text{B.int,loss}}$ = Battery internal loss
i_{BT} = Battery current
$R_{\text{B.int}}$ = Battery internal resistance

The rectifier loss is expressed as

$$P_{\text{Rec,loss}} = P_{\text{DC.PT}} \left(\frac{1}{\eta_{\text{rec}}} - 1 \right) \tag{14}$$

where

$P_{\text{Rec,loss}}$ = Rectifier loss
$P_{\text{DC.PT}}$ = Power transferred through rectifier
η_{rec} = Rectifier efficiency

The DC loads in conventional distribution systems are connected to AC terminals. The power is stepped down using transformers embedded in the appliances and converted into DC by the rectifier. Hence, feeding DC loads include the transformer loss and rectifier loss. This is expressed as follows.

$$P_{DC.load.feed} = \text{DC Demand} + P_{Rec,loss} + P_{App.trs,\ loss} \tag{15}$$

where

$P_{Rec,loss}$ = Inverter loss
$P_{App.trs,loss}$ = Appliances transformer loss

The battery power is utilized by converting to AC using an inverter; hence, the battery undergoes several loss functions before being utilized. This is expressed as

$$P_{B.feed} = \text{AC Demand} + \left(\text{DC Demand} + P_{Rec,loss} + P_{App.trs,\ loss}\right) + P_{inv,loss} + P_{B.int,loss} + P_{trs,\ loss} \tag{16}$$

To utilize the battery backup during a power outage, the inverter loss and battery internal loss need to be met before feeding the AC. Further, to meet the DC demand, the rectifier loss should also be fed.

3.2. Scheme 2: Grid-Tied Solar PV Scheme

Figure 3 presents a grid-tied rooftop PV system. The battery backup for such a system is shown separately, with a particular inverter setup. In this scheme, two converters are used, one for solar integration and the other for battery setup. Hence, the conversion losses are also doubled in this scheme.
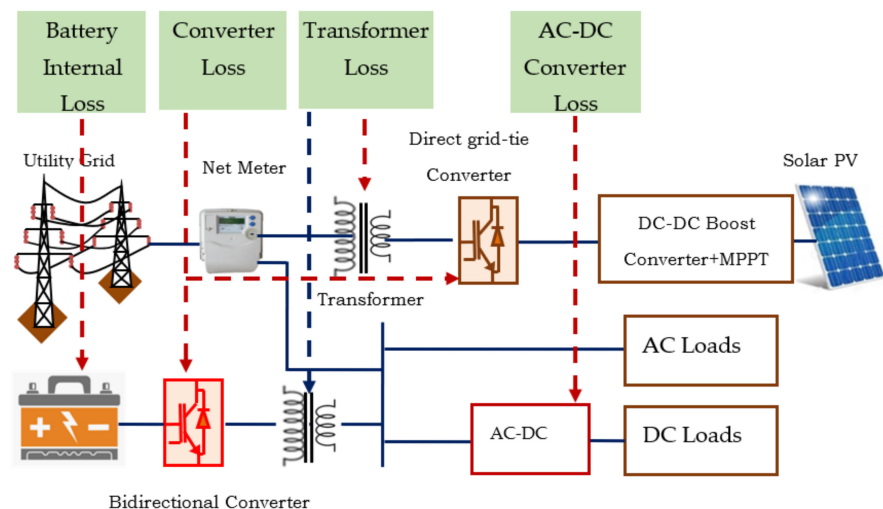
Figure 3. Direct grid-tied rooftop Solar PV with battery backup system.

In this scheme, the PV power is inverted and stepped up to a voltage to match the utility grid voltage. Hence, the PV power needs to meet both the inverter loss and the transformer loss before integrating with the grid. The power injected into the grid in this direct grid-tied rooftop Solar PV scheme feed is expressed as follows.

$$P_{ug.feed} = P_{PV} - P_{inv,loss} - P_{trs,\ loss} \tag{17}$$

3.3. Scheme 3: Solar PV Off-Grid Mode

In this scheme, the solar power is stored in the battery using a Maximum Power Point charge controller and then it is supplied to the AC busbar, where the loads are connected, using an inverter and a transformer; the schematic representation of the system is shown in Figure 4. The conversion losses, in this case, are lower when compared to the direct

grid-tied scheme. Besides, during lower load requirements or under no-load conditions, the solar power, which is generated in abundance, cannot be accommodated and is wasted.
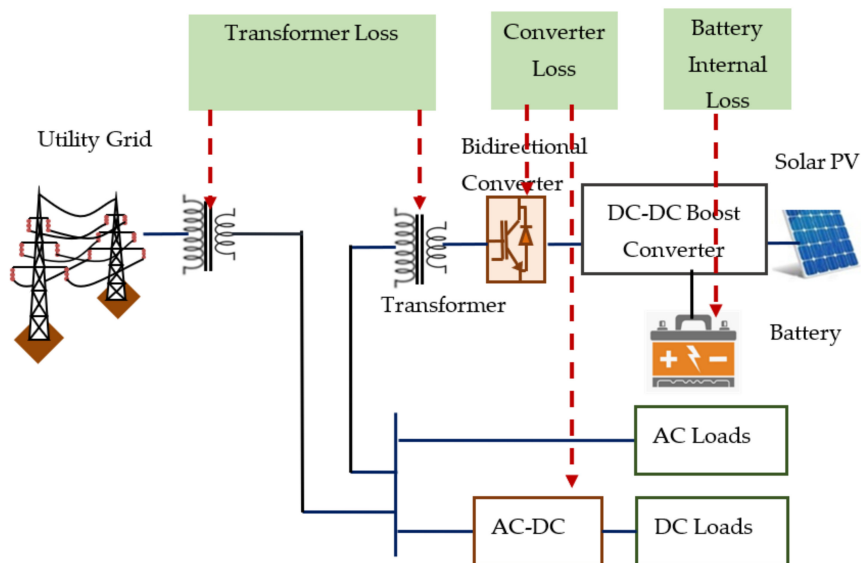
Figure 4. Solar PV off-grid system.

In this conventional off-grid mode, the solar PV power suffers inverter and transformer loss while feeding AC loads. Further, it undergoes rectifier loss to meet the DC load demand. The solar PV power utilization is expressed as follows.

$$P_{PV} = AC\ demand + P_{inv,Loss} + P_{trs,\ loss} + \left(DC\ Demand + P_{Rec,loss} + P_{App.trs,\ loss} \right) \quad (18)$$

3.4. Scheme 4: Conventional Microgrid Scheme

Figure 5 represents a microgrid system that is used for managing the AC and DC power efficiently. Still, on several occasions, the power conversion process and the losses are overcome at a greater ratio than the conventional techniques. Mainly, when storage devices such as batteries are operated in a microgrid environment, the losses increase drastically compared with conventional schemes.
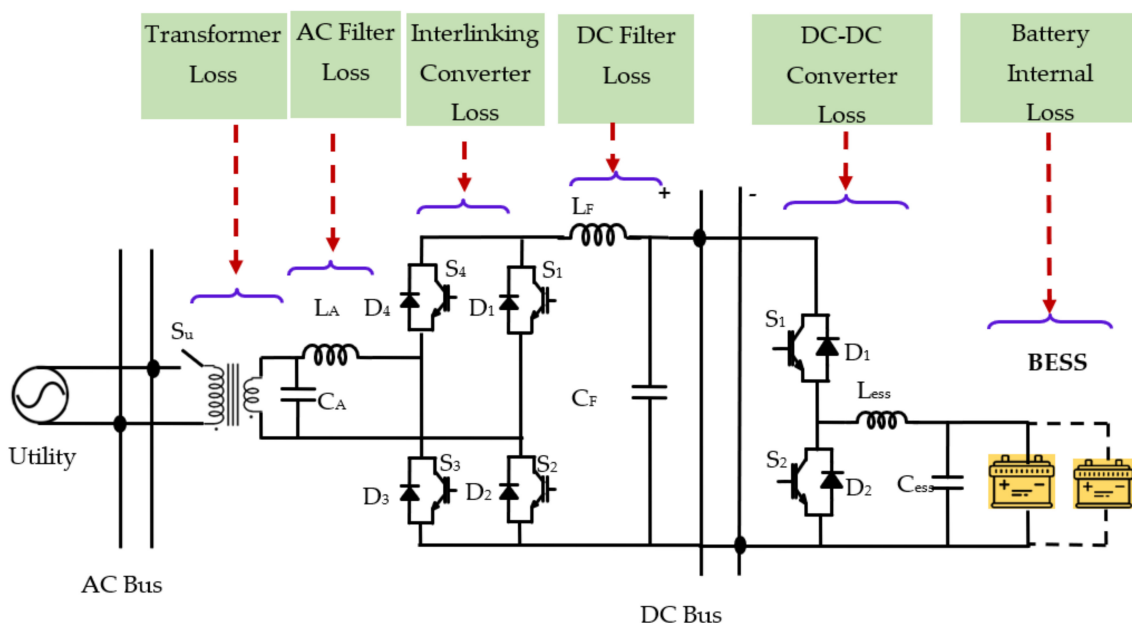
Figure 5. The losses in a microgrid with bi-directional interlinking converter configuration.

The power loss in battery storage occurs at various stages, and can be expressed as in the following equations,

$$P_{B.chg,\ loss} = P_{B.int,\ loss} + P_{dc\ conv,\ loss} + P_{rect,Loss} + P_{trs,\ loss} + P_{filt,loss} \tag{19}$$

$$P_{B.dis,\ loss} = P_{B.int,\ loss} + P_{dc\ conv,\ loss} + P_{inv,Loss} + P_{trs,\ loss} + P_{filt,loss} \tag{20}$$

where

$P_{B.chg,loss}$—Charging loss
$P_{B.dis,loss}$—Battery discharging loss
$P_{B.int,loss}$—Battery internal loss
$P_{inv,loss}$—Inverter loss
$P_{dc\ conv,loss}$—DC-DC converter loss
$P_{rect,Loss}$—Rectifier loss
$P_{trs,loss}$—Transformer loss
$P_{filt,loss}$—Filter loss

Whenever the battery is fully charged, it consumes a low current to maintain its charge level. Hence, the transformer and the inverter are under-loaded most of the time, and on several occasions, they are lightly loaded by the users. In this case, these converters and transformers drain enormous amounts of power and result in significant power loss, but this phenomenon remains unnoticed. The elimination of power conversion below 20% of the rated power is defined as an inefficient power conversion elimination strategy in this study.

4. Hybrid Microgrid System Description

A renewable energy-based hybrid microgrid configuration for the realization of the proposed IPCEA is shown in Figure 6. The AC loads are connected to the AC bus and are fed by an AC source (utility power). The DC bus of the microgrid comprises Solar PV, batteries, and DC loads. The power generated from solar PV is managed at MPP and stored using a dedicated battery when necessary. The battery bank is connected for load management and to feed the DC load during the absence of solar and utility power. Consequently, if the battery's state of charge reaches less than 50%, then the power is driven from the utility. The expression for SoC of the battery is as below.

$$SoC = \left(1 - \frac{1}{Q} \int I_B dt\right) \tag{21}$$

where

SoC—Battery State of Charge
Q—Battery Capacity
I_B—Battery Current

The incorporation of renewable energy sources, such as solar PV, plays a vital role in conversion loss reduction. Primarily, the conversion loss while feeding the DC load demand is greatly reduced. It can be expressed as follows.

During DC Demand > P_{PV}

$$P_{DC.load.feed} = (DC\ Demand - P_{PV}) + P_{DC.PT}\left(\frac{1}{\eta_{rec}} - 1\right) + P_{AC.PT}\left(\frac{1}{\eta_{App.inv}} - 1\right) \tag{22}$$

During DC Demand < P_{PV}

$$P_{DC.load.feed} = P_{PV} - DC\ Demand \tag{23}$$
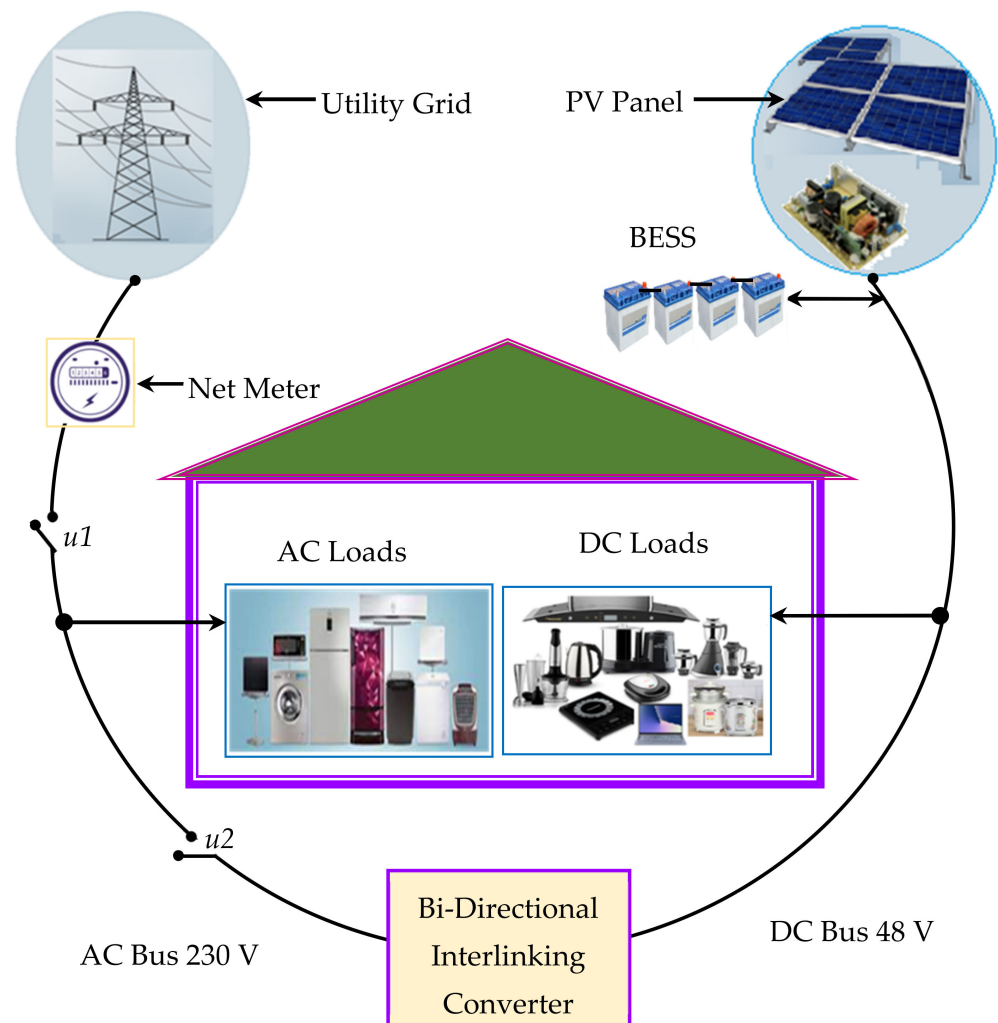
Figure 6. Hybrid microgrid system configuration.

From Equation (23), it can be inferred that the loss across the rectifier and the loss due to the appliance transformer can be eliminated by including solar PV power.

Similarly, when the battery is charged using solar power, the majority of the loss-causing factors can be avoided. This is expressed as

$$P_{B.chg,\ loss} = P_{B.int,\ loss} + P_{dc\ conv,\ loss} \tag{24}$$

Equation (24) indicates that battery charging includes only internal loss and DC converter loss, since it is charged directly from Solar PV DC power. The rectifier loss, transformer loss, and appliance transformer loss are eliminated.

4.1. Proposed Microgrid Controller Configuration

Intelligent energy management of the microgrid-based residential distribution system is done performed using a microgrid controller. The schematic of the controller is depicted in Figure 7.
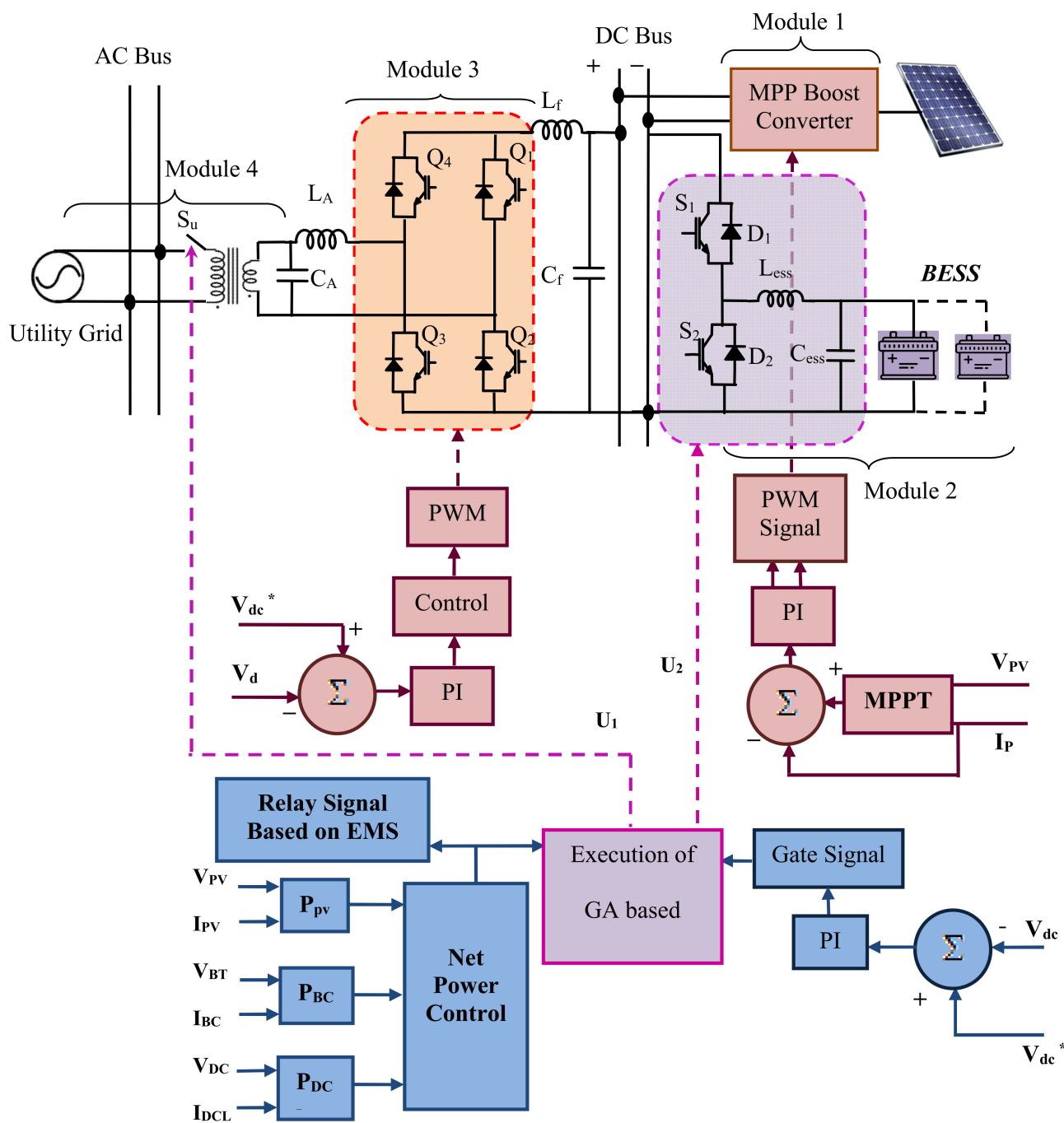
Figure 7. Schematic diagram of the hybrid microgrid controller.Parameters used in Figure 7.

Q_1, Q_2, Q_3, Q_4—Bidirectional interlinking converter IGBT switches
S_1, S_2,—Bidirectional DC converter IGBT switches
D_1, D_2,—Bidirectional DC converter diodes
V_{PV}—Solar PV voltage
I_{PV}—Solar PV current
P_{PV}—Solar PV power
V_{BT}—Battery voltage
I_{BC}—Battery current
P_{BC}—Battery power
I_{dcl}—DC load current
P_{dcl}—DC load power

V_{dc}—DC link voltage
$V_{dc}{}^{*}$—Reference DC link voltage
S_u—Utility grid voltage
L_A—AC side filter inductor
C_A—AC side filter capacitor
L_f—DC link filter inductor
C_f—DC link filter capacitor
L_{ess}—Battery side filter inductor
C_{ess}—Battery side filter capacitor
BESS—Battery energy storage system

The controller comprises four modules, as follows:

Module 1: A controller for MPP boost converter control. The Perturb and Observe algorithm is used for MPP of the solar PV system. The solar panel current I_{PV} and voltage V_{PV} values are fed into the controller and switching gate pulses are generated to operate the DC–DC boost converter.

Module 2: Comprises the controller for managing the auxiliary battery charges. The control signal is generated by comparing the reference DC bus voltage with the actual bus voltage. The bidirectional battery side converter is switched on and off depending on the optimal time of use required by the genetic algorithm.

During battery charging mode, the converter acts as a buck converter. The S_1 and D_2 conduct until the battery charges to its specified voltage. The duty cycle of the switch S_1 is obtained using the following expression.

$$\delta = \frac{V_{BT}}{V_{DC}} \tag{25}$$

where

δ = Duty cycle
V_{BT} = Battery voltage
V_{DC} = Microgrid DC bus voltage

During discharging mode, S_2 and D_1 conduct and the duty cycle of the switch S_2 is obtained using the expression

$$\delta = \frac{V_{BT} - V_{DC}}{V_{BT}} \tag{26}$$

Module 3: Consists of a controller for bidirectional interlinking converter control. It is operated with the power available at the DC side voltage profile, based on the requirement of the interlinking converter operated either as a rectifier or as an inverter. The inverter is committed to functioning based on the utility side switch S_U operation.

The bidirectional converter output voltage is controlled using the modulation index and it is expressed as follows.

$$m_a = \frac{V_{control}}{V_{triangle}} \tag{27}$$

where

m_a = Modulation index
$V_{control}$ = Voltage obtained from controller
$V_{triangle}$ = Triangular carrier wave voltage

The converter output is injected into the utility grid at an appropriate angle, which is obtained using the expression

$$\varphi = \sin^{-1}\left(\frac{\omega_1 \, L_A \, I_{AC}}{V_{AC}}\right) \tag{28}$$

where

ϕ = Angle at which voltage is injected into utility grid
L_A = AC side smoothing inductor
V_{AC} = AC voltage at inverter terminal

The power injected to the utility grid is expressed as

$$P_{AC} = \frac{V_{AC} \; V_{ug} \; \sin \varphi}{\omega_1 \; L_A} \tag{29}$$

where:

V_{ug} = Utility grid voltage
Sin ϕ = Sine of angle between inverter voltage and utility grid voltage

Module 4: The utility side switch Su is operated with an intelligent control. The interlinking converter works only if the utility switch S_U is on. The switching pattern is obtained using the genetic algorithm.

4.2. Design Procedure of the IPCEA Based Microgrid EMS

The IPCEA algorithm is based on a lower threshold limit for power transfer to avoid inefficient power transfer. The limit is set as 20% of the converter rating since the transformer connected in the circuit exhibit low efficiency when supplied less than 20% of its rating [18–20]. The converter performance is reduced by up to 52.3% when it is loaded below than this threshold. It attains a considerable level only when it is loaded more than 20% (tested experimentally and inferred in Section 2). A logical block diagram representation of the IPCEA algorithm is shown in Figure 8.
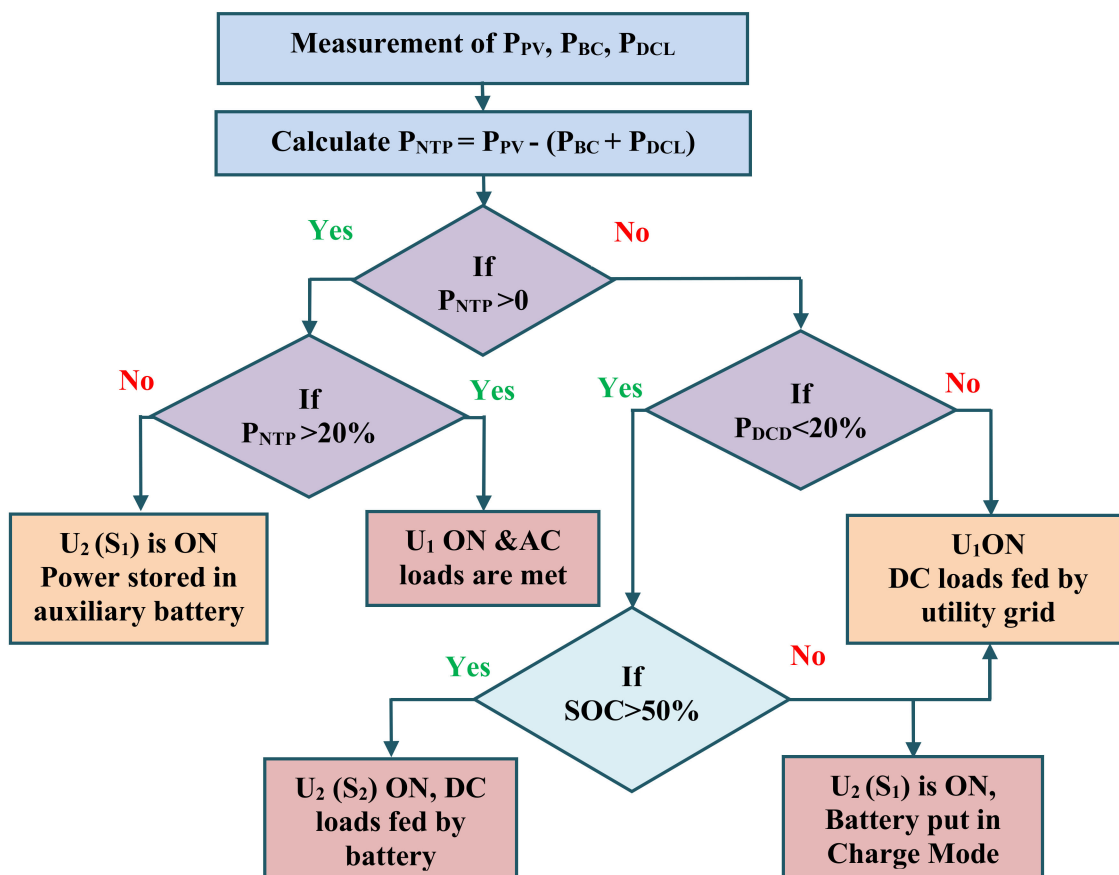

Figure 8. Logical block diagram representation of the IPCEA algorithm.

The solar PV power generation, load demand, and battery SoC are given as the input. The P_{NTP}, Net Transferable Power (NTP) at DC bus after feeding DC loads, and the BESS demand are obtained, and the expression is shown below.

$$P_{NTP} = P_{pv} - (P_{BC} + P_{DCL}) \tag{30}$$

where

P_{NTP}—Net transferable power at DC side
P_{PV}—Power from PV array
P_{BC}—Battery Charging Power
P_{DCL}—DC power load demand

If P_{NTP} is positive and greater than 20%, then the U_1 is switched ON and the solar power from the DC side is fed into the AC bus to meet the AC load demand. The import or export of power within the utility grid is performed based on the load requirement and P_{NTP} availability. If P_{NTP} is not sufficient, then U_2 (T_1) is turned ON. Here, the Power (known to be inefficient) is fed into an auxiliary battery for storage. P_{NTP} is checked if is less than zero; if this is valid, we check whether the power required by the DC side is less than 20% of the converter rating (meager requirement). If this is the case, then the DC loads are fed from the battery storage if the SoC is above 50%. A level of 50% SoC is considered safe enough to avoid deep discharge [26,27]. Hence, if the SoC is found to be less than 50%, then the utility power is drawn to meet the DC-side load demand. If the DC side demands more than 50%, power is driven from the utility grid by switching ON the switch U_1. In this case, the converter works as a rectifier in this operation mode.

4.3. Genetic Algorithm for Cost Minimization

The IPCEA can minimize the conversion losses effectively, but to reduce energy costs in the region with a time-of-use tariff system requires the optimization of energy distribution. In this study, a Genetic Algorithm (GA)-based optimization technique was used for cost reduction. This was achieved in four steps.

Step 1: The input parameters include instantaneous solar PV power, AC- and DC-side load demand, and the battery's state of charge.
Step 2: Calculation of NTP using Equation (10) and load demands using real-time data.
Step 3: Execution of the genetic algorithm.

The objective function of the system for cost minimization is defined as

$$MinJ = \sum_{t=0}^{T} P_{GS}(t) * C_{GS}(t) \tag{31}$$

$$P_{GS}(t) = P_{ACD}(t) + P_{Conv}u_1 + P_{DCD}(t) + P_{BL}(t)u_2 - P_{PV}(t) \tag{32}$$

where

P_{GS}—Grid-side power
C_{GS}—Cost of the grid power
P_{ACD}—AC-side power demand
P_{Conv}—Power loss across converter
P_{DCD}—DC-side power demand
P_{BL}—Power loss across battery
P_{PV}—Power from PV array

where u_1 is the switching command to operate the switch S_U to connect the AC and DC buses for power transfer. Its value is

$$u_1 = \begin{cases} 1 \\ 0 \end{cases}$$

u$_2$ is the switching command to connect the battery with the DC bus, which takes the value

$$u_2 = \begin{cases} 1 & \text{Chargingmode} \\ 0 & \text{Float mode} \\ -1 & \text{Dischargingmode} \end{cases}$$

The modes are operated in the following format:

Charging Mode: The battery is placed in charging operation mode where S$_1$ and D$_2$ conducts; the battery charges to the required level.

Float Mode: In this mode, the battery does not exchange power with the network. It merely stays connected in the line. Further, it receives a minimum current to maintain the charge in its state.

Discharging Mode: In this mode, S$_2$ and D$_1$ conduct and the battery power is utilized to meet the load demand. The S$_2$ modes are enabled concerning the SoC of the battery.

The constraints used for achieving cost minimization and inefficient power conversion reductions are as follows:

- SOC limits: $90\% > SoC(t) > 50\%$
- Power transfer switch u$_1$ enabled if $P_{NTP} \& P_{DCD} > 20\%\ of\ P_{CR}$
- When $P_{NTP} < 20\%$ and $P_{DCD} < 20\%$, switch u_2 is enabled to access the battery power.

The flow diagram of the genetic algorithm used for the realization of IPCEA is shown in Figure 9. GA is used to optimize the power distribution in the microgrid such that the electricity cost is minimized.
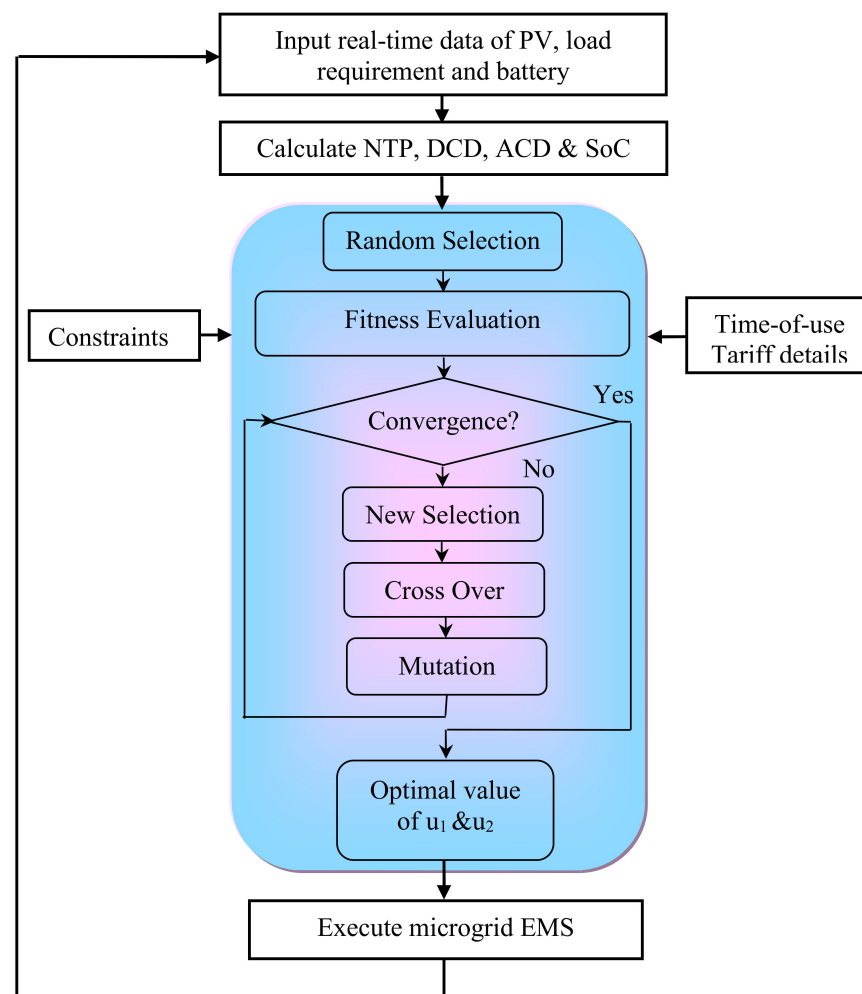
Figure 9. Flow chart of the GA-based microgrid energy management system.

The GA execution is as follows:

- Selection of population (random, size = 50).
- Fitness evaluation (Individual).
- Check for criterion satisfaction.
- If the condition is not satisfied, another new population set is selected (roulette wheel selection).
- Go for cross-over (single cross-over).
- The mutation rate is fixed as 0.2.
- Check for convergence.

Step 4: Execution of microgrid energy management.

The developed control algorithm generates a reference signal based on the threshold limits and the actual power availability for microgrid energy management. It produces control signals to actuate the converter operation during power transfer. Further, it delivers power transfer with the utility grid.

5. Comparative Investigation

This discussion considers a comparative investigation of the conventional direct grid-tied solar PV scheme and a conventional microgrid system. In this paper, a detailed comparative analysis was performed to exhibit the effectiveness of the proposed hybrid microgrid system as well as the significance of the IPCEA algorithm. The investigation includes real-time data of solar PV. The location-based solar PV data were obtained from NREL [28], and the domestic load data was extracted on an hourly basis from the web [29]. The average residential DC load demand was approximately 40%. It comprised electronic gadgets, lighting, and fan loads. The AC load demand was considered to be 60%, as inferred from [30,31]. The detailed data set used in this study is outlined in Table 1. The power consumption pattern of the conventional domestic distribution scheme, which uses a direct grid-tied solar PV system, is shown in Table 2. The generated solar power is fully transferred to the grid using a direct grid-tied converter in the conventional scheme and the power required for domestic loads is drawn from the utility grid.

Table 1. Hourly solar PV power generation and averaged domestic load consumption details.

| | | | | | Loads Categorized under Microgrid System | |
Time (h)	Ambient Temperature (°C)	Irradiance (W/m^2)	DC Array Output (W)	Hourly Load Consumption at Conventional Distribution System (W)	DC side Load Consumption (W)	AC side Load Consumption (W)
	(NREL's PV Watts Calculator) [23]			(State Load Dispatch Centre) [24]	Considered 40% DC Loads and 60% AC Loads [25,26]	
0	22.244	-	-	192.085	76.834	115.251
1	21.765	-	-	175.315	70.126	105.189
2	21.331	-	-	164.895	65.958	98.937
3	20.965	-	-	164.895	65.958	98.937
4	20.625	-	-	192.085	76.834	115.251
5	20.326	-	-	240.105	96.042	144.063
6	22.105	-	-	381.04	152.416	228.624

Table 1. *Cont.*

Time (h)	Ambient Temperature (°C)	Irradiance (W/m²)	DC Array Output (W)	Hourly Load Consumption at Conventional Distribution System (W)	Loads Categorized under Microgrid System	
					DC side Load Consumption (W)	AC side Load Consumption (W)
(NREL's PV Watts Calculator) [23]				(State Load Dispatch Centre) [24]	Considered 40% DC Loads and 60% AC Loads [25,26]	
7	25.699	176.492	140.983	432.19	172.876	259.314
8	28.928	462.707	360.468	434.375	173.75	260.625
9	31.457	749.333	538.987	478.125	191.25	286.875
10	33.336	918.126	632.724	480.21	192.084	288.126
11	34.627	1015.382	706.22	432.19	172.876	259.314
12	35.253	1037.075	715.193	384.165	153.666	230.499
13	35.293	975.038	677.895	356.98	142.792	214.188
14	34.83	830.184	590.165	343.75	137.5	206.25
15	33.729	624.961	456.195	335.415	134.166	201.249
16	32.034	381.406	279.857	336.46	134.584	201.876
17	29.391	144.65	107.653	356.98	142.792	214.188
18	27.59	-	-	384.165	153.666	230.499
19	26.339	-	-	367.395	146.958	220.437
20	25.211	-	-	336.145	134.458	201.687
21	24.232	-	-	308.96	123.584	185.376
22	23.496	-	-	260.94	104.376	156.564
23	22.892	-	-	215.21	86.084	129.126

Table 2. Power consumption pattern of direct grid-tied solar PV-based commonly used conventional domestic distribution scheme.

Time (h)	Hourly Load Consumption (W)	Solar Power Output (W)	Solar Power Delivered to the Grid after Conversion (W)	Power Loss across Converter (W)
0	192.085	-	-	-
1	175.315	-	-	-
2	164.895	-	-	-
3	164.895	-	-	-
4	192.085	-	-	-
5	240.105	-	-	-
6	381.04	-	-	-
7	432.19	140.983	62.850	78.133
8	434.375	360.468	233.475	126.993

Table 2. *Cont.*

Time (h)	Hourly Load Consumption (W)	Solar Power Output (W)	Solar Power Delivered to the Grid after Conversion (W)	Power Loss across Converter (W)
9	478.125	538.987	395.670	143.317
10	480.21	632.724	482.262	150.462
11	432.19	706.22	549.934	156.287
12	384.165	715.193	558.137	157.056
13	356.98	677.895	523.877	154.018
14	343.75	590.165	442.978	147.187
15	335.415	456.195	319.519	136.676
16	336.46	279.857	164.751	115.105
17	356.98	107.653	43.277	64.377
18	384.165	-	-	-
19	367.395	-	-	-
20	336.145	-	-	-
21	308.96	-	-	-
22	260.94	-	-	-
23	215.21	-	-	-
Total	7754.075	5206.34	3776.730	1429.610

Note: Certain values are shaded to highlight the period when the inefficient conversion occurred.

The limitation considered in this scheme is the fact that the generated DC power from the solar PV is inverted every time before feeding to the grid. If the power available at the solar PV terminal is inefficient i.e., less than 20% of the converter rating, the power transfer leads to enormous conversion losses. Hence, to overcome the limitations of the conventional solar PV scheme, the microgrid-based power distribution possess certain advantages. The power consumption pattern of the conventional microgrid-based power distribution scheme with solar PV is depicted in Table 3. The DC and AC distribution buses can be built to feed the loads separately. The DC power generated from the solar PV can be fed directly to DC loads without much conversion. The solar power is only active for six hours a day, and the remaining part of the AC power must be converted to feed DC loads.

Similarly, solar power is inverted to feed AC loads when it is abundant. Hence, the system undergoes redundant conversion, which leads to high conversion losses. Further, inefficient power conversion was encountered in the microgrid power distribution system. The portion of this inefficient power conversion period is shown below, using color shading.

5.1. Realization of the GA for Cost Minimization

GA-based optimization was used to minimize the conversion loss and cost. It was mainly used in the time-of-use tariff system. The time-of-use tariff detail is depicted in Table 4.

Table 3. Power consumption pattern of solar PV-equipped conventional microgrid-based power distribution scheme.

Time (h)	DC load Demand(W)	AC Load Demand (W)	Solar Power Availability (W)	Solar Power Available at DC Bus after Feeding DC Loads (W)	Solar Power Available at AC Side after Conversion (W)	Power Required to Supply DC Loads Including Conversion loss (W)	Total Power-Driven from the Utility Grid (W)	Power Exported to the Grid (W)	Power Loss across Converter (W)
0	76.83	115.25	-	-	-	90.39	205.64	-	13.56
1	70.13	105.19	-	-	-	82.50	187.69	-	12.38
2	65.96	98.94	-	-	-	77.6	176.54	-	11.64
3	65.96	98.94	-	-	-	77.6	176.54	-	11.64
4	76.83	115.25	-	-	-	90.39	205.64	-	13.56
5	96.04	144.06	-	-	-	112.99	257.05	-	16.95
6	152.42	228.62	-	-	-	169.35	397.98	-	16.94
7	172.88	259.31	140.98	-	-	37.52	296.84	-	5.63
8	173.75	260.63	360.47	186.72	93.27	-	167.4	-	93.45
9	191.25	286.88	538.99	347.74	222.34	-	64.53	-	125.4
10	192.08	288.13	632.72	440.64	305.36	-	0	17.24	135.28
11	172.88	259.31	706.22	533.34	390.46	-	0	131.15	142.88
12	153.67	230.5	715.19	561.53	416.49	-	0	185.99	145.04
13	142.79	214.19	677.9	535.10	392.07	-	0	177.88	143.03
14	137.5	206.25	590.17	452.67	316.32	-	0	110.07	136.34
15	134.17	201.25	456.2	322.03	200.11	-	1.140	-	121.92
16	134.58	201.88	279.86	145.27	65.53	-	136.34	-	79.740
17	142.79	214.19	107.65	-	-	41.34	255.53	-	6.20
18	153.67	230.5	-	-	-	170.74	401.24	-	17.07
19	146.96	220.44	-	-	-	163.29	383.72	-	16.33
20	134.46	201.69	-	-	-	149.4	351.09	-	14.94
21	123.58	185.38	-	-	-	137.32	322.69	-	13.73
22	104.38	156.56	-	-	-	115.98	272.54	-	11.6
23	86.08	129.13	-	-	-	101.28	230.40	-	15.19
						Total	4490.49	622.33	1320.43

Note: Certain values are shaded to highlight the period when inefficient conversion occurred.

Table 4. Time-of-use tariff detail.

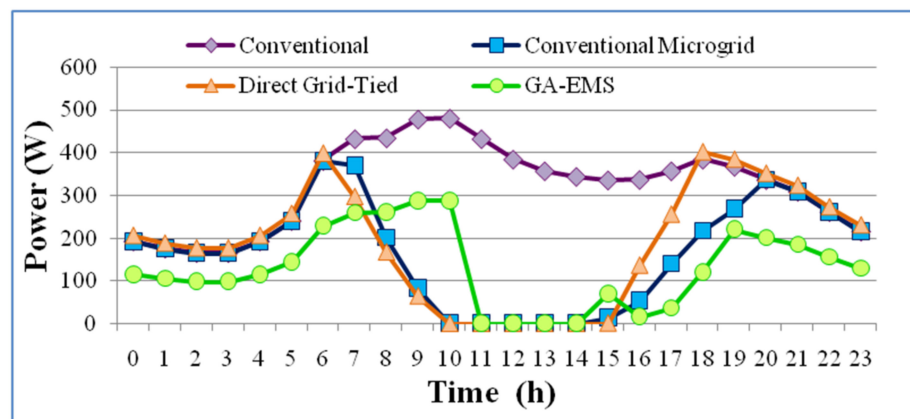| Time	Tariff (Rs)
0–6	4
7–10	6
11–16	5
17–22	6
23–24	4

Advisory Control Output

A genetic algorithm was executed, resulting in the cost function's convergence; it is shown in Figure 10. The switching pattern was obtained using GA optimization and the values of u_1 and u_2 are depicted as follows:

$$u_1 = [0\,0\,0\,0\,0\,0\,0\,0\,0\,0\,0\,0\,1\,1\,1\,1\,0\,0\,0\,0\,0\,0\,0\,0]$$

$$u_2 = [1\ 1\ 1\ 1\ 1\ 1\ 1\ 1 - 1 - 1 - 1\ 0\ 0\ 0\ 0 - 1 - 1\ 1\ 1\ 1\ 1\ 1\ 1\ 1]$$

Figure 10. Convergence of cost function by iteration.

To initiate power transfer across the interlinking converter, the pattern u_1 has been used; pattern u_2 has been used to manage the battery energy for obtaining the optimal energy cost. This can be observed in Figure 11.

Figure 11. Switching patterns u_1 and u_2.

5.2. Conversion Loss Reduction Strategy of the Proposed Scheme

A unique solution was obtained using the proposed IPCEA-based energy management strategy. The solar PV was connected to the DC bus of the microgrid and met the DC load demand. The batteries were used to handle the DC loads in the absence of solar power. The battery capacities were selected based on the DC load requirement. The batteries were charged using solar PV power when the solar power generation was active, and the backup was used during its absence.

Further, as per the proposed algorithm, inefficient power was utilized for maximally charging the battery. This scheme of power distribution reduced the conversion process significantly, and inefficient conversion was eliminated. The proposed IPCEA-based microgrid-supported power distribution scheme is summarized in Table 5. The conversion efficiency can be observed in Figure 1. The power driven from utility throughout the day for all the schemes is represented in Figure 12. Figure 13 highlights the importance of the proposed algorithm for reducing conversion losses.

Table 5. Power consumption pattern of proposed IPCEA-based microgrid-supported power distribution scheme.

Time Period (h)	DC Load Consumption (W)	AC Load Consumption (W)	Solar Power Available at DC Bus after Feeding DC Loads (W)	Solar Power Fed to Battery for Charging (W)	Solar Power Transferred to AC Terminals after Conversion (W)	DC Power Required at DC Terminals Fed by Battery (W)	Net Power-Driven from the Utility Grid (W)	Power Exported to the Grid (W)	Power Loss across Converter (W)
0	76.83	115.25	-	-	-	76.834	115.251	-	-
1	70.13	105.19	-	-	-	70.126	105.189	-	-
2	65.96	98.94	-	-	-	65.958	98.937	-	-
3	65.96	98.94	-	-	-	65.958	98.937	-	-
4	76.83	115.25	-	-	-	76.834	115.251	-	-
5	96.04	144.06	-	-	-	96.042	144.063	-	-
6	152.42	228.62	-	-	-	152.42	228.624	-	-
7	172.88	259.31	-	-	-	31.893	259.314	-	-
8	173.75	260.63	186.72	186.72	-	-	260.63	-	-
9	191.25	286.88	347.74	347.74	-	-	286.875	-	-
10	192.08	288.13	440.64	440.64	-	-	288.126	-	-
11	172.88	259.31	533.34	-	390.464	-	-	131.15	142.883
12	153.67	230.5	561.53	-	416.485	-	-	185.99	145.04
13	142.79	214.19	535.10	-	392.07	-	-	177.88	143.03
14	137.5	206.25	452.67	-	316.32	-	-	110.07	136.34
15	134.17	201.25	322.03	322.03	-	-	201.25	-	-
16	134.58	201.88	145.27	145.27	-	-	201.88	-	-
17	142.8	214.19	-	-	-	35.14	214.19	-	-
18	153.67	230.5	-	-	-	153.67	230.5	-	-
19	146.96	220.44	-	-	-	146.96	220.44	-	-
20	134.46	201.69	-	-	-	134.46	201.69	-	-
21	123.58	185.38	-	-	-	123.58	185.38	-	-
22	104.38	156.56	-	-	-	104.38	156.56	-	-
23	86.08	129.13	-	-	-	86.084	129.13	-	-
					Total		3742.2	605.09	567.3

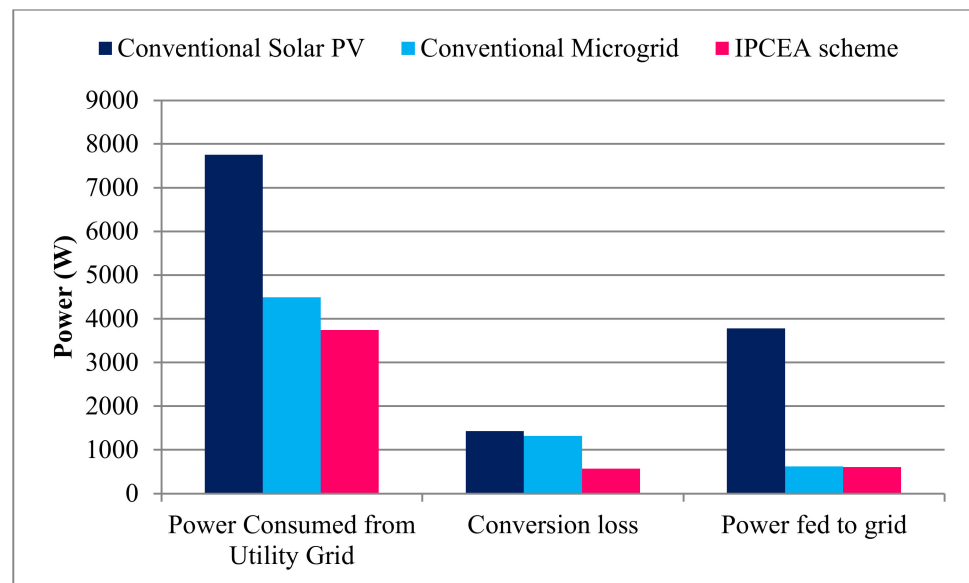**Figure 12.** Power driven from the utility.

Figure 13. Power exchange and conversion loss comparison chart.

The hourly energy cost of each scheme was set using the time-of-use tariff rate. The monthly electricity cost was evaluated for various schemes considered for this investigation, and the comparison details are recapitulated in Table 6. Further elaboration of the cumulative energy savings and cost reduction per month for the various schemes is presented in Table 7.

Table 6. Cost of electricity drawn by various schemes.

Time Period (h)	Conventional Scheme		Conventional Solar PV Scheme		Conventional Microgrid EMS Scheme		Proposed GA Based EMS Scheme	
	Hourly Load Consumption (W)	Cost of Electricity (Rs)	Hourly Load Consumption (W)	Cost of Electricity (Rs)	Total Power Driven from Utility Grid (W)	Cost of Electricity (Rs)	Net Power Driven from Utility Grid (W)	Cost of Electricity (Rs)
0	192.09	0.77	192.09	0.77	205.64	0.82	115.25	0.46
1	175.32	0.70	175.32	0.70	187.69	0.75	105.19	0.42
2	164.90	0.66	164.90	0.66	176.54	0.71	98.94	0.40
3	164.90	0.66	164.90	0.66	176.54	0.71	98.94	0.40
4	192.09	0.77	192.09	0.77	205.64	0.82	115.25	0.46
5	240.11	0.96	240.11	0.96	257.05	1.03	144.06	0.58
6	381.04	1.52	381.04	1.52	397.98	1.59	228.62	0.91
7	432.19	2.59	369.34	2.22	296.84	1.78	259.31	1.56
8	434.38	2.61	200.90	1.21	167.36	1.00	260.63	1.56
9	478.13	2.87	82.46	0.49	64.53	0.39	286.88	1.72
10	480.21	2.88	0.00	0.00	0.00	0.00	288.13	1.73
11	432.19	2.16	0.00	0.00	0.00	0.00	0.00	0.00

Table 6. *Cont.*

Time Period (h)	Conventional Scheme		Conventional Solar PV Scheme		Conventional Microgrid EMS Scheme		Proposed GA Based EMS Scheme	
	Hourly Load Consumption (W)	Cost of Electricity (Rs)	Hourly Load Consumption (W)	Cost of Electricity (Rs)	Total Power Driven from Utility Grid (W)	Cost of Electricity (Rs)	Net Power Driven from Utility Grid (W)	Cost of Electricity (Rs)
12	384.17	1.92	0.00	0.00	0.00	0.00	0.00	0.00
13	356.98	1.78	0.00	0.00	0.00	0.00	0.00	0.00
14	343.75	1.72	0.00	0.00	0.00	0.00	0.00	0.00
15	335.42	1.68	13.84	0.07	1.14	0.01	70.10	0.35
16	336.46	1.68	53.97	0.27	136.34	0.68	15.89	0.08
17	356.98	2.14	139.73	0.84	255.53	1.53	36.31	0.22
18	384.17	2.30	217.27	1.30	401.24	2.41	120.43	0.72
19	367.40	2.20	268.17	1.61	383.72	2.30	220.44	1.32
20	336.15	2.02	336.15	2.02	351.09	2.11	201.69	1.21
21	308.96	1.85	308.96	1.85	322.69	1.94	185.38	1.11
22	260.94	1.57	260.94	1.57	272.54	1.64	156.56	0.94
23	215.21	0.86	215.21	0.86	230.40	0.92	129.13	0.52
Total	7754.08	40.88	3977.35	20.35	4490.49	23.13	3137.11	16.67

Table 7. Comparison of beneficial features of the proposed scheme.

Schemes	Net Power Consumed from Utility Grid/Month	Energy Savings due to Solar PV/Month	Electricity Charges/Month
Conventional scheme	232,622.3	-	1226.527
Direct Grid-Tied Solar PV scheme	119,320.4	130,306.8	610.35
Conventional Microgrid EMS scheme	134,714.8	154,842.6	693.9154
Proposed GA based scheme	94,113.21	153,023.7	499.9768

6. Discussion and Conclusions

From the results presented in Table 7, it can be observed that when applied in the energy management of distribution system, the proposed IPCEA strategy results in the reduction of power conversion loss and paves an optimum approach to energy conservation. The conventional rooftop solar PV scheme provided a 48.7% reduction in electricity consumption from the utility grid, whereas the proposed scheme provided a 59.54% decrease in power consumption. Further, the conventional solar PV scheme and the GA-based energy management approach decreased the electricity cost by 50.23% and 59.23%, respectively.

The extensive experimental analyses and literature survey evidently proved that the conversion loss is tremendous in a conventional distribution system and in conventional solar PV deployment schemes. Moreover, the existing microgrid scheme also suffered

conversion losses on several occasions. Inefficient power conversion took place more frequently in the microgrid scheme than in the conventional scheme.

The proposed IPCEA-based hybrid microgrid energy management system significantly reduced conversion losses as well as minimizing energy costs. The approach also enhanced the energy economy of the domestic power distribution system. Inefficient power conversion was eliminated, which resulted in significant power savings. The battery's energy storage and distribution were managed within the DC bus, and multiple conversion processes were curtailed. Further, the proposed energy management system reduced solar PV grid interaction issues by avoiding ineffective grid exchanges.

Appendix A

Particulars	Specification
Model	UPSEB 900 VA (12)
Rated Capacity	800 VA
Output Power	672 Watts
Input Voltage	100–300 V
Efficiency	84%
Charging Current	10 Amps
Product Dimensions	38.1 cm $\times$ 35.6 cm $\times$ 20.3 cm
Weight	10 kg

References

1. Rodriguez-Otero, M.A.; O'Neill-Carrillo, E. Efficient home appliances for a future DC residence. In Proceedings of the 2008 Energy 2030 Conference, Atlanta, GA, USA, 17–18 November 2008; pp. 17–18.
2. Foster Porter, S.; Denkenberger, D.; Mercier, S.; May-Ostendorp, P. Reviving the War of Currents: Opportunities to Save Energy with DC Distribution in Commercial Buildings. *Proc. ACEEE Summer Study Energy Effic. Build.* **2014**, *85*, 3.
3. Mahmoud, M.S. *Microgrid Advanced Control Methods and Renewable Energy System Integration*; Hayton, J., Ed.; Elsevier: Cambridge, MA, USA, 2017; pp. 1–42.
4. Hirsch, A.; Parag, Y.; Guerrero, J. Microgrids: A review of technologies, key drivers, and outstanding issues. *Renew. Sustain. Energy Rev.* **2018**, *90*, 402–411. [CrossRef]
5. Ramli, M.A.M.; Bouchekara, H.R.E.H.; Alghamdi, A.S. Efficient Energy Management in a Microgrid with Intermittent Renewable Energy and Storage Sources. *Sustainability* **2019**, *11*, 3839. [CrossRef]
6. Longe, O.M.; Ouahada, K.; Rimer, S.; Ferreira, H.C.; Han Vinck, A.J. Distributed Optimisation Algorithm for Demand Side Management in a Grid-Connected Smart Microgrid. *Sustainability* **2017**, *9*, 1088. [CrossRef]
7. Silva, G.F.; Donaire, A.; Seron, M.M.; Aaron McFadyen, A.; FordString, J. Stability in Microgrids Using Frequency Controlled Inverter Chains. *IEEE Control Syst. Lett.* **2021**, *6*, 1484–1489. [CrossRef]
8. Zheng, L.; Kandula, R.P.; Divan, D. Current-Source Solid-State DC Transformer Integrating LVDC Microgrid, Energy Storage, and Renewable Energy into MVDC Grid. *IEEE Trans. Power Electron.* **2021**, *37*, 1044–1058. [CrossRef]
9. Lee, E.-K.; Shi, W.; Gadh, R.; Kim, W. Design and Implementation of a Microgrid Energy Management System. *Sustainability* **2016**, *8*, 1143. [CrossRef]

10. Takahashi, M.; Nishijima, K.; Nagao, M.; Sato, T.; Nabeshima, T. A Hybrid Converter for Improving Light Load Efficiency. *IEEJ Trans. Ind. Appl.* **2011**, *13*, 1007–1012. [CrossRef]

11. Jens, F.; Leon, F. Efficiency Optimization for Partial Load Operation of Interleaved Converters. In Proceedings of the 23rd International Conference on Electrical Machines and Systems (ICEMS), Hamamatsu, Japan, 24–27 November 2020.

12. Li, C.; Jia, X.; Zhou, Y.; Li, X. A microgrids energy management model based on multi-agent system using adaptive weight and chaotic search particle swarm optimization considering demand response. *J. Clean. Prod.* **2020**, *262*, 121247. [CrossRef]

13. Iqbal, S.; Nasir, M.; Zia, M.F.; Riaz, K.; Sajjad, H.; Khan, H.A. A novel approach for system loss minimization in a peer-to-peer energy sharing community DC microgrid. *Int. J. Electr. Power Energy Syst.* **2021**, *129*, 106775. [CrossRef]

14. Lenhart, S.; Araujo, K. Microgrid decision-making by public power utilities in the United States: A critical assessment of adoption and technological profiles. *Renew. Sustain. Energy Rev.* **2021**, *139*, 110692. [CrossRef]

15. Yanine, F.; Sanchez-Squella, A.; Barrueto, A.; Parejo, A.; Cordova, F.; Rother, H. Grid-tied distributed generation systems to sustain the smart grid transformation: Tariff analysis and generation sharing. *Energies* **2020**, *13*, 1187. [CrossRef]

16. Gangatharan, S.; Rengasamy, M.; Elavarasan, R.M.; Das, N.; Hossain, E.; Sundaram, V.M. A Novel Battery supported Energy Management System for the effective handling of Feeble power in Hybrid Microgrid Environment. *IEEE Access* **2020**, *8*, 217391–217415. [CrossRef]

17. Mageswaran, R.; Sivasankar, G.; Rajvikram, M.E.; Mihet-Popa, L. The Motivation for Incorporation of Microgrid Technology in Rooftop Solar Photovoltaic Deployment to Enhance Energy Economics. *Sustainability* **2020**, *12*, 10365. [CrossRef]

18. How to Determine Transformer Efficiency? Electrical Engineering. Available online: https://www.engineeringenotes.com/electrical-engineering/transformer/how-to-determine-transformer-efficiency-electrical-engineering/27945 (accessed on 23 March 2021).

19. What Is the Effect of under Load Transformer for Energy Losses? Electrical Engineering. Available online: https://www.researchgate.net/post/what_is_the_effect_of_underload_transformer_for_energy_losses (accessed on 16 June 2021).

20. Suresh, K.; Devishree, J. Evaluation of transformer loading and energy loss for increasing energy efficiency in distribution system. In Proceedings of the 12th International Conference on Electrical Engineering/Electronics, Computer, Telecommunications and Information Technology (ECTI-CON), Hua Hin, Thailand, 24–27 June 2015.

21. Notton, G. Hybrid wind-photovoltaic energy systems. In *Stand-Alone and Hybrid Wind Energy Systems Technology, Energy Storage and Applications*; Woodhead Publishing Series in Energy; Elsevier: Amsterdam, The Netherlands, 2010; pp. 216–253. [CrossRef]

22. Hakans, A.; Ugur, S.S. Hybrid switch use for light load efficiency improvement of a power inverter for stand-alone residential renewable energy system. In Proceedings of the 15th European Conference on Power Electronics and Applications (EPE), Lille, France, 2–6 September 2013.

23. Hina, F.; Prabaharan, N.; Palanisamy, K.; Akhtar, K.; Saad, M.; Jackson, J.J. *Hybrid-Renewable Energy Systems in Microgrids*; Woodhead Publishing: Chicago, IL, USA, 2018; pp. 23–37.

24. Charging and Discharging Lead Acid Batteries. Available online: https://www.solar-facts.com/batteries/battery-charging.php (accessed on 24 March 2021).

25. Characteristics of Lead Acid Batterie. Available online: https://www.pveducation.org/pvcdrom/lead-acid-batteries/characteristics-of-lead-acid-batteries (accessed on 24 March 2021).

26. Zeh, A.; Müller, M.; Naumann, M.; Hesse, H.; Jossen, A.; Witzmann, R. Fundamentals of Using Battery Energy Storage Systems to Provide Primary Control Reserves in Germany. *Batteries* **2016**, *2*, 29. [CrossRef]

27. Hesse, H.C.; Schimpe, M.; Kucevic, D.; Jossen, A. Lithium-Ion Battery Storage for the Grid—A Review of Stationary Battery Storage System Design Tailored for Applications in Modern Power Grids. *Energies* **2017**, *10*, 2107. [CrossRef]

28. NREL (National Renewable Energy Laboratory). PVWatts ®Calculator. Available online: https://pvwatts.nrel.gov (accessed on 6 April 2021).

29. State Load Dispatch Centre, Delhi. Available online: https://www.delhisldc.org/Loadcurve.aspx (accessed on 6 April 2021).

30. Glasgo, B.; Azevedo, I.L.; Hendrickson, C. How much electricity can we save by using direct current circuits in homes? Understanding the potential for electricity savings and assessing feasibility of a transition towards DC powered buildings. *Appl. Energy* **2016**, *180*, 66–75. [CrossRef]

31. Garbesi, K.; Vossos, V.; Shen, H. *Catalog of DC Appliances and Power Systems*; Lawrence Berkeley National Laboratory: Berkeley, CA, USA, 2010.